# The Moon as a Calibration Load for the Breadboard Array

D. Morabito,[1] M. Gatti,[2] and H. Miyatake[2]

*The calibration of radio antenna performance is a well-understood process. For system noise measurements in the current Deep Space Network (DSN), a noise diode is used along with an ambient absorber that is placed over the feed to make a direct measurement of the system noise as well as to characterize the diode. For future arrays, consisting of a large number of antennas, it will be necessary to minimize the amount of hardware, electronics, and time spent on each antenna. This work describes an effort to use the moon as the standard calibrator for the system noise injection diode. This work was inspired by the recent demonstration of consistency of very accurate pre-existing lunar brightness temperature maps, physical optics characterization of the 34-m beam-waveguide antenna patterns, and Moon-centered measurements at the DSN's research and development antenna, DSS 13. The brightness temperature maps and antenna patterns were convolved to yield expected antenna temperatures for comparison with the Moon-centered observations. Due to limitations caused by atmospheric effects, the absolute calibration of the system diode will have larger error bounds as compared with the use of an ambient aperture load. However, results are very adequate for rapid, ongoing checks of the health and noise level of the receiving system. We describe the proposed method as used on the DSN Array breadboard antennas, with results and error analyses.*

## I. Introduction

Arrays of smaller-diameter antennas have been proposed to provide future capability in the Deep Space Network (DSN). Simple, highly reliable antennas have been proposed for this purpose. The DSN is evaluating whether or not to eventually replace its monolithic large-diameter antennas with these arrays in order to realize equivalent or greater $G/T$ performance[3] [1] for downlink and equivalent or greater effective isotropic radiated power (EIRP) for uplink. A breadboard array consisting of two 6-m-diameter antennas and one 12-m-diameter antenna has been developed and deployed on the Mesa Antenna Range located in the foothills above JPL. The 12-m antenna employs Cassegrainian optics whereas the 6-m antennas employ Gregorian optics. The 12-m-diameter antenna is a prototype for a future array[4] whose

[1] Communications Architectures and Research Section.

[2] Communications Ground Systems Section.

[3] $G/T$ is a measure of antenna system performance; it is the ratio of antenna gain to system noise temperature.

[4] The actual diameter for the array antennas as well as the number, configuration, and site locations are yet to be determined.

The research described in this publication was carried out by the Jet Propulsion Laboratory, California Institute of Technology, under a contract with the National Aeronautics and Space Administration.

signals can be combined to realize an equivalent $G/T$ of a single larger structure. The purpose of this breadboard is to investigate and characterize radio frequency (RF), signal processing, interferometry, signal combining, and monitor and control aspects important for arraying, as well as to characterize the performance of the 12-m antenna as an array element. Early work with the 6-m antennas included tracking the Mars Reconnaissance Orbiter (MRO) 8.4-GHz (X-band) and 32-GHz (Ka-band) signals in November 2005 during the cruise period when MRO was relatively close to the Earth [2].

The most common method for measuring the noise performance of a system during operations is to use an injected noise of a known value [3–5]. A noise diode (ND) is normally used to provide the injected signal by means of an appropriate injection port on the input side of the low-noise amplifier (LNA). The technical issue then becomes a problem of accurate calibration of the injected signal. There are several ways in which one may calibrate this injected signal, including comparison with other calibrated noise standards (e.g., noise diode signals), ambient and/or cryogenic aperture loads, and ambient waveguide loads. All of these techniques require that additional hardware be installed on the antenna. There is an interest in keeping the antennas used in a large array inexpensive. To aid in simplicity, reliability, and cost, the current design has no provision for automatically switching the input of the low-noise amplifiers into calibration standards for the purposes of noise temperature measurement. Although a noise injection diode is included in the system, its automated periodic calibration is not provided for. In the current DSN, this calibration standard is an ambient absorber placed over the microwave feed horn used to make a direct measurement of the system noise as well as to characterize a noise injection diode.

Alternatively, in order to easily characterize these noise diodes without any other hardware, a procedure using the Moon as a calibration load was devised and tested. This method is preferred over placing an ambient temperature calibrator load over the feed horn in that it is more easily accomplished, requires no extra hardware be added to the antenna (e.g., switches and loads), and can be done in a fraction of the time. This technique will have larger errors than using an aperture load, but it will be of immense help in frequent measurement of system performance. Thus, the more accurate ambient load calibration method does not have to be performed as often, and can be done occasionally to check and validate the method of using the Moon as a calibration load.

The use of this technique for the breadboard array, with the Moon serving as a calibration load, allows for checking the integrity of the system, including validating the canned-in values of the noise temperatures of the noise diodes. This provides confidence in the operational system that produces estimates of system noise temperature on a regular basis, from the validated ND noise temperature values using the Y-factor method with input linearized synchronous detector outage voltages (alternating with the ND turned-on and with the ND turned-off).

The Moon is a thermal blackbody radiator at microwave frequencies and emits radiation that varies in intensity with the lunar phase cycle at wavelengths smaller than about 5 cm (frequency = 6 GHz). The microwave radio emission signature with lunar phase exhibits a retardation of about 40 deg relative to that of the visible and infrared [6] due to latent heating of the lunar regolith at the shallow depths probed at these frequencies. The lunar phase cycle has a period of 29.5 days, the synodic period of the Moon's orbit around the Earth relative to the direction of the Sun.

As suggested before, this calibration method can be used to measure the equivalent noise temperature contribution of the noise diodes. For the breadboard array, the values of the noise diode temperatures are used in the conversion of synchronous detector output voltages to system noise temperature. This technique can also be used to check consistency of other parameters such as the equivalent temperature of the back-end equipment as seen at the input to the LNA. All three breadboard antennas were calibrated concurrently using a script file, demonstrating its potential use in the case of a large array of many antennas per complex. This method could also be used as a system integration test that can be used to verify the optics and pointing performance of the antenna system.

## II. Background

In order to estimate the expected noise temperature increase of the Moon that is required to perform calibrations, knowledge of the Moon's brightness temperature is required. Calculated brightness temperature maps of the Moon are available at X-band and Ka-band [7,8]. These maps consist of two-dimensional arrays of Earth-viewed brightness temperatures of the lunar regolith for lunar phase angles from 0 to 360 deg in steps of 12 deg. These are theoretical pencil-beam maps (models) that were generated based on thermo-physical and electrical properties of the lunar surface material derived from Apollo program findings (experiments and laboratory). These models have been validated from Earth-based measurements made in the 1960s from 1 mm to 10 cm [7,8]. The Earth-based microwave and infrared measurements have also served as constraints for developing the global-scale regolith model. These maps can be used to infer antenna response from measurements or to validate measurements using physical optics (PO) models of the antenna.

One such characterization was performed for the case of the Goldstone research and development 34-m-diameter beam-waveguide (BWG) antenna, DSS 13, at 2.3 GHz (S-band), X-band, and Ka-band. A study was conducted with the purpose of measuring the system noise temperature increase at each of these frequencies for application in future telecommunication links involving assets in orbit around the Moon or on the lunar surface [9]. The measurements of noise temperature increase with the antenna beams pointed at the center of the Moon were then compared with estimates derived from a physical optics characterization of the DSS-13 34-m-diameter BWG antenna using lunar brightness temperature maps as input [10]. It was found that the measurements agreed with the brightness model predictions after refinements to the physical optics model were implemented for the case of an extended source. For instance, holography maps of the DSS-13 antenna surface were required in order to more accurately model blockage due to the subreflector and struts [11].

A physical optics characterization was performed for the case of the 6-m- and 12-m-diameter breadboard antennas at X-band and Ka-band.[5] Estimates of the noise temperature for the 6-m- and 12-m-diameter antennas while pointed at clear sky can be found in [12,13]. The physical optics analysis for this type of calibration requires that the antenna patterns be known either from theoretical modeling or from measurements. In either case, it will be assumed that the antenna patterns are known. During other testing, it was found that the 12-m antenna as built is susceptible to thermal loads such that its patterns change from day to night. To account for this, multiple analyses were done for selected periods of the day spaced 2 hours apart. The contribution to the noise temperature due to the struts is an estimate since holographic data do not yet exist for the breadboard array antennas (unlike the case of the DSS-13 study).

Results of the physical optics analysis are shown in Figs. 1(a) and 1(b). These figures represent the expected difference in system temperatures one would measure when observing the noise temperature when the beam is pointed at the center of the lunar disk and subtracting that observed on the sky (the beam is offset several Moon widths in cross-elevation). In other words, this can be used as the value of noise measured in an ambient load calibration of the antenna. The model temperature differences in Figs. 1(a) and 1(b) are plotted as a function of lunar phase angle where 180 deg corresponds to "Full Moon" and 0 deg (or 360 deg) pertains to "New Moon." Figure 1(a) represents the expected result for lunar noise temperature increase at X-band on the 12-m antenna. Here, because the frequency is X-band, we assume that thermal distortion due to solar heating in the daytime is negligible. The Ka-band curve used for nighttime (minimal distortion of the dish) is shown in Fig. 1(b), accounting for the effect of the struts.

[5] W. Imbriale, personal communication, Jet Propulsion Laboratory, Pasadena, California, August–September 2006.

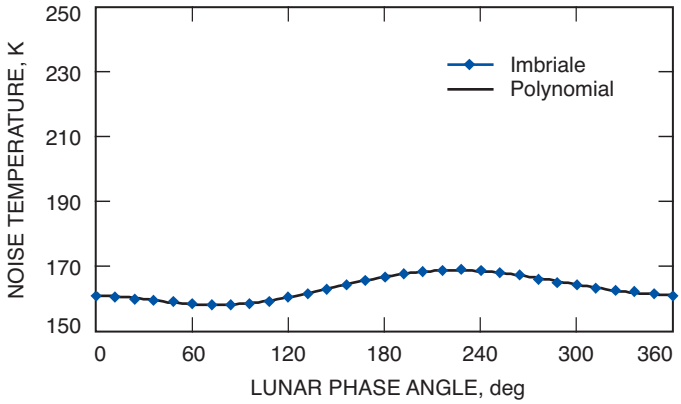


**Fig. 1(a). Lunar noise temperature increase at X-band for the 12-m-diameter antenna (points). The fitted polynomial used to model the data is also shown (solid black line).**

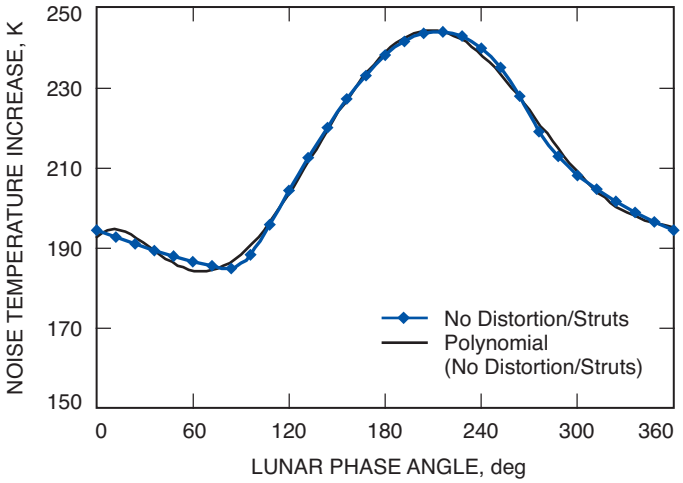


**Fig. 1(b). Lunar noise temperature increase at Ka-band for the 12-m-diameter antenna accounting for struts, with no thermal distortion (blue points). The fitted polynomial used to model the data is also shown (black solid line)**

A plot illustrating theoretical (Bessel pattern) one-dimensional cuts of the X-band and Ka-band beam patterns for the 12-m antenna against the backdrop of the Moon is provided in Fig. 2. The Moon's mean distance from the Earth is about 384,400 km. The Moon's mean radius is 1738 km (a diameter of 3476 km). Thus, the disk of the Moon on average subtends about 0.52 deg in angle. For reference, the half-power beam widths (HPBWs) for the 12-m-diameter antenna are ∼180 mdeg at X-band and ∼50 mdeg at Ka-band, and for the 6-m-diameter antenna they are ∼360 mdeg at X-band and ∼95 mdeg at Ka-band. With an orbital eccentricity of about 0.0549, the distance of the Moon from the Earth varies from about 406,000 km to 363,000 km, resulting in the Moon's angular extent varying from 0.49 to 0.55 deg. The physical optics analysis assumed the mean distance of the Moon from the Earth, and thus this effect has not been corrected for in this analysis.

The results of this study have practical applications in radio astronomy, Moon observations, and antenna calibration, replacing the standard DSN aperture load calibration. The methods described in this study can also provide measurements of system noise temperature, gain stability, receiver linearity, and injection noise diode temperature.

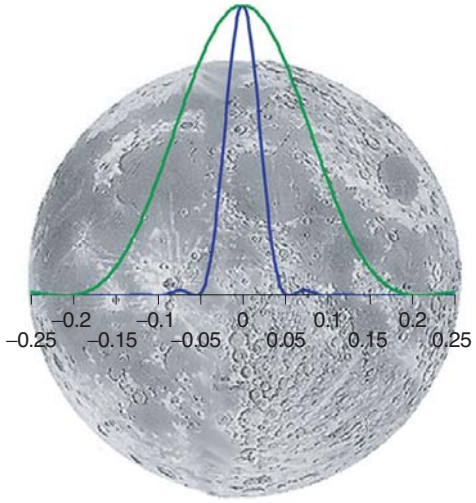


**Fig. 2. One-dimensional theoretical antenna pattern slices for X-band (green) and Ka-band (blue) projected against the Moon for the 12-m-diameter antenna (units in degrees).**

## III. Equipment Description

The 12-m and 6-m antennas of the prototype breadboard array are shown in Figs. 3(a) and 3(b), respectively. Figure 4 presents the block diagram of the electronics equipment that is utilized in the breadboard array. The single cryogenic front-end contains the feed and LNA for both the X-band and Ka-band signals. Each frequency band includes dual-channel LNAs, each one provided signals from one each of the two signals output from a circular polarizer. The diode detectors allow for power measurements that are needed in order to perform various functions. With information obtained from calibrations, the power measurements can be converted to system noise temperature. Noise diode signals can be injected into the LNAs to accommodate real-time performance characterization of the system. The injected noise either may be always on or off or may be modulated at a frequency of 80 Hz. This allows for easy estimation of system noise temperature from the synchronous detector output, given that all of the calibration information has been programmed in advance (linearization coefficients and noise diode values). The LNA bias (LNB) module (Fig. 4) provides bias voltages for the LNAs. The noise calibration (NCAL) module (Fig. 4) provides control signals to the noise diodes, turning them on or off, or modulating them per received control directives.

Follow-on back-end equipment allows for frequency downconversion from RF frequencies to intermediate frequency (IF) frequencies centered at 960 MHz. Referring to Fig. 4, the downconversion is accomplished from the local oscillator receiver (LORX) board that provides mixing signals to the X-band conversion (XCON) electronics. These mixing signals are produced by phase-locked oscillators driven by reference signals derived from a maser frequency reference provided over stabilized fiber optics by the Frequency and Timing Laboratory at JPL. The signals are routed to dual-channel IF processors (IFTX in Fig. 4) that include the synchronous detectors. The synchronous detectors output voltage levels that are ideally linearly proportional to the input power levels, but in practice have a non-linearity that requires characterization. This non-linearity can be characterized by performing calibrations over a wide range of noise temperature values. Varying attenuator values (from 0 to 31.5 dB) also can be used. Such calibrations can be performed using an ambient load covering the feed packages. The difference between sky and ambient load temperature allows for determination of coefficients that correct for linearization.

(a)

(b)

**Fig. 3. Antennas at JPL: (a) 12-m-diameter antenna and (b) 6-m-diameter antennas.**

A wide range of attenuation settings can be applied to the input of the dual-channel IF processor to allow for varying input signal levels. The applied attenuation can range from 0 to 31.5 dB in half-decibel steps.

There are filters in the RF chain and in the IF chain that can be used to set the equivalent bandwidth of the received signals. The available RF filter selections for Ka-band (centered at 32,000 MHz) include a through path with no filter, and a path with a 1200-MHz filter. For X-band, the available RF filter selections include a 1200-MHz and a 200-MHz path. In the IF section, filtering can be selected from either a 700-MHz or a 200-MHz filter.

The signals at the output of the synchronous detectors then are recorded using appropriate sampling and integration times. The recorded voltages and their uncertainties (scatters) from the synchronous detectors then are written onto files that can be imported into applications such as Microsoft Excel for further analysis. Since these antennas are part of an array, the signals from each antenna front-end also can be combined using specialized signal-processing software and equipment [14].

## IV. Calibration Approach

The calibration approach involves using a technique developed by Charles Stelzried and Michael Klein for the DSN [15] involving the use of a power meter and ambient load. However, in this analysis, we replace the aperture load with the Moon, and we replace the power meter with the synchronous detector. Since the lunar noise temperature will vary as a function of lunar phase, the physical optics–derived model temperatures were fit as a function of lunar phase using a polynomial [see the solid black curves in Figs. 1(a) and 1(b)]. For routine implementation, a future model may use Fourier coefficients instead of the polynomial. The coefficients of these fits then are implemented in the algorithm, which produces the lunar noise temperature for the particular value of lunar phase for the observation. The controlling script file extracts this value of lunar phase from the ephemeris run that is used to generate the pointing file for the pass. The pointing coordinates are generated using the JPL Solar System Dynamics (SSD) Horizons

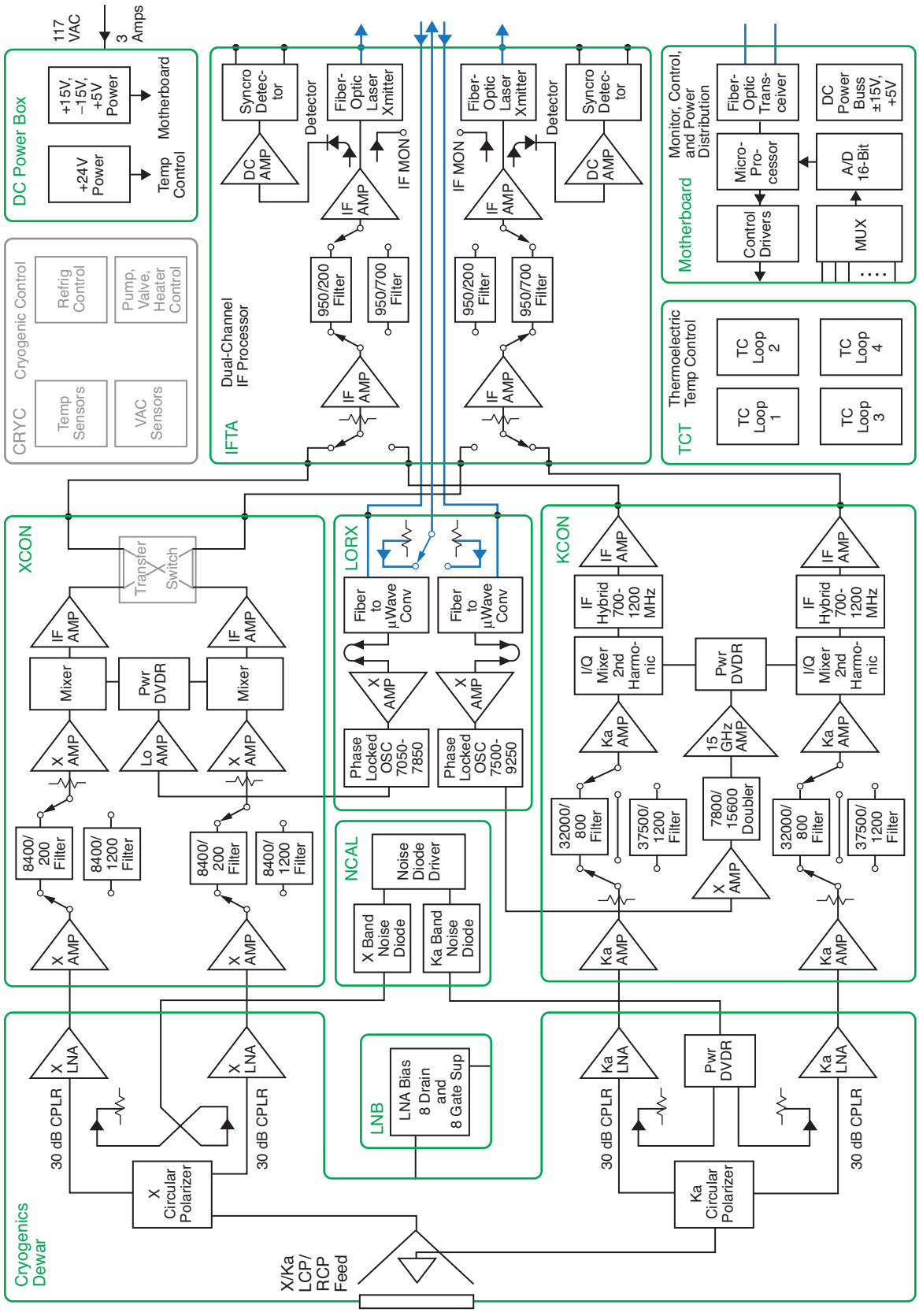


**Fig. 4. System block diagram of electronics equipment.**

program [16–18]. During the measurement session, antenna tipping curves also are performed sufficiently far away from the Moon (5 deg in cross-elevation). The tipping curves can be used to estimate (or check) the contribution of the equipment temperature referenced at the feed horn aperture, and the optical depth of the atmosphere at zenith. The follow-up equipment temperature is understood to also include effects due to any radio frequency interference (RFI) and spillover. Alternatively, the zenith optical depth also can be estimated from a weather model using surface meteorological data as input.[6]

The calibration sequence includes performing measurements with the antenna beam centered on the Moon and with the antenna beam moved sufficiently far off of the Moon so as to ensure that only cold sky noise temperature is measured, free of any contribution from the lunar disk (see Fig. 5). The difference of these two quantities provides the raw noise temperature increase $\Delta T$ due to the Moon. Figure 6 illustrates the basic concept in the idealized case where the relationship is linear.

The measurements typically were performed for each of the following front-ends:

Antenna 1 6-m X-band right circular polarization (RCP)

Antenna 2 6-m X-band RCP

Antenna 3 12-m X-band RCP

Antenna 1 6-m Ka-band left circular polarization (LCP)

Antenna 2 6-m Ka-band LCP

Antenna 3 12-m Ka-band LCP

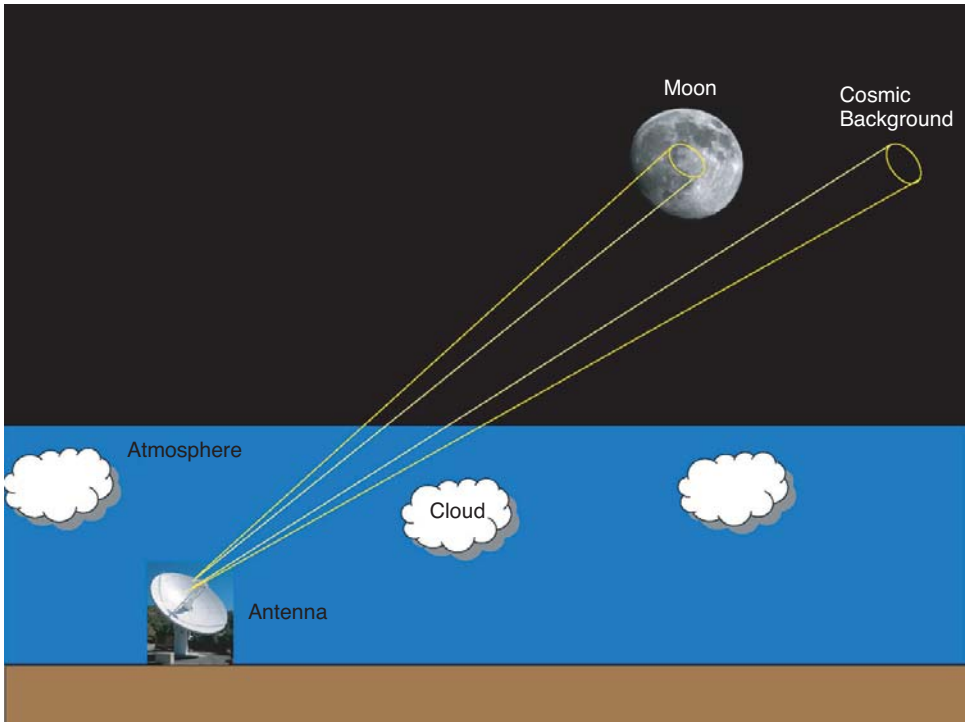


**Fig. 5. Cartoon depicting the lunar-ambient load calibration method. The antenna cycles between lunar disk center and cold sky background. Moon photo credit: NASA/GSFC/ METI/ERSDAC/JAROS, and U.S./Japan ASTER Science Team.**

[6] S. Slobin, personal communication, Jet Propulsion Laboratory, Pasadena, California, 2006.

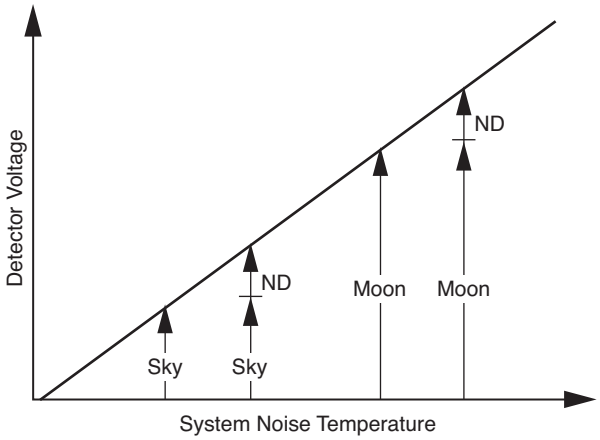


**Fig. 6. Diagram illustrating the ideal linear relationship between detector voltage and system noise temperature with the antenna on (1) cold sky, (2) cold sky with noise diode (ND) turned on, (3) Moon, and (4) on the Moon with ND turned on.**

The sequence thus involves observing the synchronous detector voltage for the following measurements along with the state of the noise diode (ND), performed simultaneously for each antenna front-end (see Fig. 6):

V1: Sky, antenna offset 5 deg in cross-elevation, ND off

V2: Sky + ND, antenna offset 5 deg in cross-elevation, ND on

V3: Moon, antenna beam centered on the Moon, ND off

V4: Moon + ND, antenna beam centered on the Moon, ND on

In addition, additional measurements are taken on-source and off-source but with the diode modulated at a frequency of 80 Hz and using the synchronous detector to measure the diode for consistency-check purposes. As previously stated, tip curve sequences are alternated with the lunar calibration measurements.

This measurement at each position consists on sampling the detector voltage for 150 ms once each second and taking 7 samples of the voltage and outputting the mean and scatter. The antenna then is moved to the next position, where about 7 seconds are used to allow the detector output voltage to settle prior to sampling the next measurement. The filters used for each front-end are configured such that they provide an equivalent noise bandwidth of 700 MHz for both X-band and Ka-band systems.

The system noise temperature for each state described above then can be represented using a model as follows:

$$
\begin{aligned}
T1M &= T_{\rm equip} + T_{\rm phys}\left(1 - e^{-\tau/\sin(\theta)}\right) + T_{\rm cosmic}/e^{\tau/\sin(\theta)} + T_{\text{sp-rfi}}(\theta) \\
T2M &= T1M + T_{ND} \\
T3M &= T_{\rm equip} + T_{\rm phys}\left(1 - e^{-\tau/\sin(\theta)}\right) + T_{\rm Moon}(\phi)/e^{\tau/\sin(\theta)} + T_{\text{sp-rfi}}(\theta) \\
T4M &= T3M + T_{ND}
\end{aligned}
$$

where

$T_{\text{Moon}}(\phi) =$ noise temperature increase due to the Moon with the antenna beam centered on the lunar disk for the value of lunar phase, $\phi$, during the pass (K). This is extracted from a physical optics analysis–derived model of W. Imbriale[7] (see Figs. 1(a) and 1(b) for the case of the 12-m antenna).

$T_{\text{equip}} =$ noise temperature of follow-up receiver electronics equipment referenced to the feed horn aperture, accounting for contributions due to the antenna, LNA, and follow-up equipment (K).

$T_{\text{sp-rfi}} =$ noise temperature effects such as spillover and radio frequency interference (K).

$T_{\text{phys}} =$ physical temperature of the atmosphere (280 K, single layer).

$T_{\text{ND}} =$ noise diode temperature (K).

$\tau =$ optical depth of the atmosphere at zenith as measured by a tip curve or estimated from the surface weather model[8] using surface meteorological measurements as input.

$\theta =$ antenna beam elevation angle.

$\phi =$ lunar phase angle of the observation.

The calibration is performed using the output voltage of the synchronous detector when in non-modulation mode, with the noise diode either turned on or turned off. A linearization is performed (assuming the DC bias term is small and can be neglected) using the Stelzried and Klein method [15]:

$$CC = \frac{V4 - V3 - V2 + V1}{V3(V4 - V3 - V2 + V1) - (V4^2 - V3^2 - V2^2 + V1^2)}$$

$$BC = 1 - CC\ V3$$

Using the derived CC and BC coefficients above, we can then calculate the corrected detector voltages as follows:

$$V1C = BC \times V1 + CC \times V1^2$$

$$V2C = BC \times V2 + CC \times V2^2$$

$$V3C = BC \times V3 + CC \times V3^2 = V3$$

$$V4C = BC \times V4 + CC \times V4^2$$

The model-derived temperature with the antenna beam centered on the Moon's disk, $T3M$, is used to set the scale factor of the system as follows:

$$G = \frac{T3M}{V3}$$

[7] W. Imbriale, op cit.

[8] S. Slobin, op cit.

The gain for each measurement cycle can be normalized by the gain value from the first cycle, thus allowing gain stability to be characterized during the period of the calibrations.

This gain is then applied to each of the other synchronous detector voltages measured during the present cycle:

$$T1C = G\ V1C$$

$$T2C = G\ V2C$$

$$T3C = G\ V3 = T3$$

$$T4C = G\ V4C$$

The noise diode temperature then can be estimated as follows:

$$T_{\mathrm{ND}} = T2C - T1C$$

$$T_{\mathrm{ND}} = T4C - T3$$

Given a linear system, the noise diode temperature $T_{\mathrm{ND}}$, estimated from either $T2C - T1C$ or $T4C - T3$, should be essentially identical.

Uncertainties in the estimation of the noise diode temperature can be inferred from

(1) uncertainties of the raw detector voltage, which can be estimated from the scatter on the individual voltage measurement over the cycle time, and

(2) uncertainties in the model temperature used to set the system gain.

We expect that a certain amount of uncertainty is due to the linearization; however, the linearization should remove a significant systematic error that would have been in place had not the linearization been performed.

There should be some degree of error due to neglecting the DC bias term in the linearization process, which can be estimated or bounded (discussed later).

The error in the detector voltage $\sigma_V$ is deduced from the scatter of the measurements over several cycles. The uncertainty in the model temperature $T3$, which sets the system gain for each cycle, is given by

$$\sigma_{T3} = \sqrt{\sigma^2_{T\mathrm{equip}} + \sigma^2_{T\mathrm{atm}} + \sigma^2_{T\mathrm{sp\text{-}rfi}} + \sigma^2_{\mathrm{Moon}}} \tag{1}$$

We can neglect systematic errors for now, which are estimated to be about 5 percent for all front-ends, except for FE32 (Antenna 3 Ka-band), where the error is about 10 percent (not including thermal distortion).

The random error over a measurement cycle for $T3$ (on the Moon) will be dominated by the atmosphere, which can vary from below 0.1 K (at X-band) to a few tenths of a kelvin (at Ka-band). We assume that the calibration measurements are usually performed during clear weather conditions.

The uncertainty (or random noise) on the estimate of the noise diode temperature contribution is given by

$$\sigma_{T\mathrm{ND}} = \sqrt{\sigma_{T4C}^2 + \sigma_{T3}^2}$$

where

$$\sigma_{T4C} = T4C\sqrt{\left(\frac{\sigma_G}{G}\right)^2 + \left(\frac{\sigma_{V4C}}{V4C}\right)^2} \tag{2}$$

and where

$$\sigma_{V4C} = (BC + 2\ CC\ V4)\,\sigma_{V4}$$

Thus, the expected random noise for the estimate of noise diode temperature is thought of as being due to two principal terms. One is directly measured from repeated samples ($T3$) and the other ($T4C$) is a model whose noise is estimated from known fluctuating noise sources (atmosphere and system gain). The system gain contribution to the noise can be extracted from the time series on normalized gain stability over the time scales of interest.

The gain stability over a measurement cycle period (∼30 seconds) can vary but is nominally about $\sigma_G/G \sim 0.001$. This happens to be about the same order as the relative voltage error, which can include gain fluctuations as well as atmospheric fluctuations $\sigma_{\mathrm{V4C}}/\mathrm{V4C} \sim 0.001$. The random noise contribution on $T4C$, inferred from Eq. (2), is projected to be about 0.1 K to 0.3 K under most normal conditions. This value is comparable to the noise on the modeled values of the system noise temperature while pointed at the Moon, explainable by the various random error contributors (atmosphere, gain instability, etc.) [see Eq. (1)].

The effect of not including DC bias voltages in the algorithm was found to be negligible using DC offset values available from Bardin[9] in modified versions of the equations. Here the results using a maximum value of the DC bias voltage versus the case of not using a DC bias voltage (zero) were compared. However, it is cautioned that, even though the DC bias voltages are periodically monitored, they could attain higher values in future configurations.

## V. Results

Over the course of several months, several data acquisition passes using the Moon, of several hours duration each, were conducted in order to test the calibration technique described in Section IV. An example of normalized system gain and its variation during the course of a several-hour track on 2006/306 (denoting year 2006 and day of year 306, corresponding to November 2, 2006) is shown in Fig. 7.

For nominal system noise temperatures with the antenna beam centered on the Moon ($T4C \sim 150$ K), the variation in system gain over a measurement cycle ($\sigma_G/G \sim 0.001$) translates to about $\sigma_{T4C} \sim 0.2$ K.

[9] J. Bardin, *Diode Detector Square Law Correction*, JPL internal report, Jet Propulsion Laboratory, Pasadena, California, January 19, 2005.

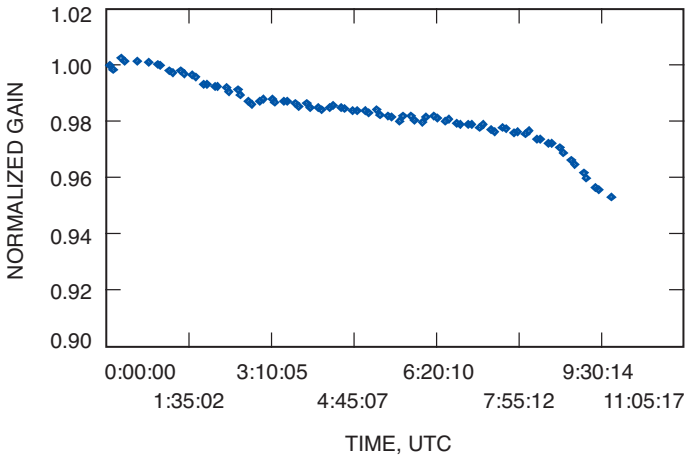


**Fig. 7. Example of normalized system gain for the case of Ka-band on the 12-m antenna during the 2006/306 pass.**

The variation in normalized system gain can be inferred upon close inspection of the scatter of repeated measurements over the time scale of interest in Fig. 7. Gain stability over the several-hour periods of most passes was generally good, within 1 percent, and even better on shorter time periods within each pass.

An example of the noise diode value estimates and its scatter can be inferred from an inspection of Fig. 8 for the case of X-band RCP on Antenna 1 for the measurement session on 2006/306. Noise diode value estimates and scatter for the case of Ka-band LCP on Antenna 1 for the measurement session performed on 2006/306 are shown in Fig. 9. The estimates of noise diode temperature at X-band RCP on the 12-m-diameter antenna from measurement calibrations performed on 2007/019 (January 19, 2007) are shown in Fig. 10.

Figure 11 displays the system noise temperature values obtained using different methods when Antenna 3 (12-m-diameter antenna) is pointed on the center of the lunar disk (on-source) and while pointed on the cold sky (off-source). Note that values obtained using Bardin coefficients[10] and default noise diode values (blue dots) are biased significantly higher than those using the other method while pointed on the Moon. The cold-sky values are closer in agreement although there is high scatter of several kelvins, presumably due to amplified error due to linearization (the gain is set by the on-source Moon temperatures while the noise diode is turned off, thus projecting variations onto the off-source noise temperature values).

The summary for the analysis of the lunar noise data for X-band RCP on the 12-m-diameter Antenna 3 is shown in Table 1. The default ND temperature value (except where noted otherwise) used for comparison for the first few passes (2.45 K) is from Weinreb.[11] The front-ends for Antennas 1 and 3 were switched on January 11, 2007. The data for the last pass in Table 1 were acquired using the 12-m antenna with the front-end equipment relocated from Antenna 1. An ambient-load/sky calibration was performed[12] on January 18, 2007 and the resulting noise diode value is provided in the table for 2007/019. This value of 2.177 K agrees well with the value obtained from the lunar noise temperature calibration data (2.18 K), where the 0.003-K difference falls well within the scatter of the measurements (0.07 K).

[10] Ibid.

[11] S. Weinreb, *DSAN RF Electronics*, Microwave Array Project MMR (JPL internal document), Jet Propulsion Laboratory, Pasadena, California, November 2005.

[12] L. D'Addario and H. Miyatake, personal communication, Jet Propulsion Laboratory, Pasadena, California, 2007.

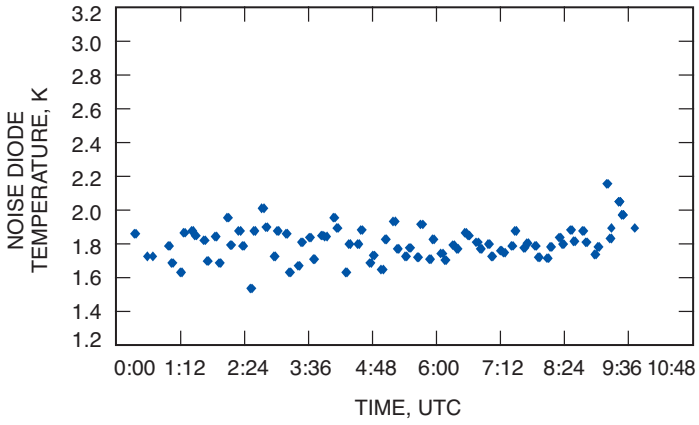


**Fig. 8. Noise diode measurements at X-band RCP on the 6-m-diameter antenna from lunar noise calibrations performed on 2006/306.**

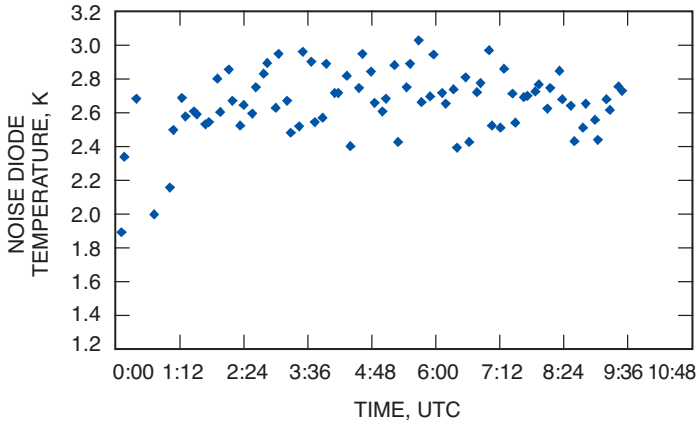


**Fig. 9. Noise diode measurements at Ka-band LCP on the 6-m-diameter antenna from lunar noise calibrations performed on 2006/306.**

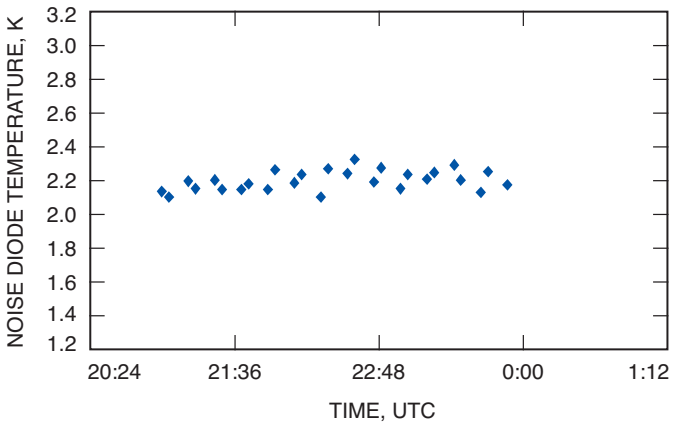


**Fig. 10. Noise diode measurements at X-band RCP on the 12-m-diameter antenna from lunar noise calibrations performed on 2007/019.**

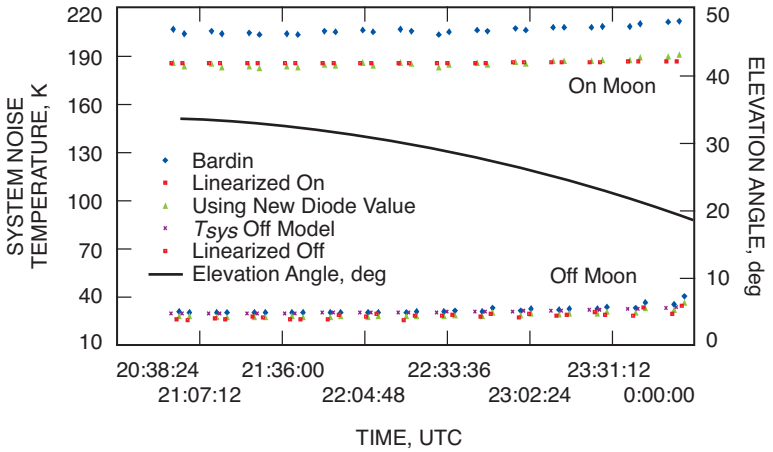


**Fig. 11. System noise temperature and elevation angle profile for X-band RCP data acquired during pass 2007/019 using the 12-m-diameter antenna.**

**Table 1. X-band RCP summary on Antenna 3 (12 m).**

| Pass | Time span, UTC | Lunar phase angle, deg | $T_{ND}$ mean, K | $T_{ND}$ scatter, K | $T_{ND}$ default, K | $T_{ND}$ error, K | $T_{ND}$ error/ scatter | Gain stab., % | CC mean | CC st. dev. | BC mean | BC st. dev. | $T_{equip}$, K | $\tau$ zenith |
|---|---|---|---|---|---|---|---|---|---|---|---|---|---|---|
| 2006/306 | 00:04–09:43 | 152.01 | 2.36 | 0.07 | 2.45 | −0.09 | −1.29 | 0.6 | 0.0181 | 0.0066 | 0.8654 | 0.0492 | 17.0 | 0.0126 |
| 2006/313 | 07:04–17:00 | 212.76 | 2.38 | 0.11 | 2.45 | −0.07 | −0.64 | 0.5 | 0.0182 | 0.0080 | 0.8609 | 0.0620 | 18.3 | 0.0128 |
| 2006/320 | 11:36–13:57 | 330.03 | 2.37 | 0.08 | 2.45 | −0.08 | −1.00 | 0.7 | 0.0145 | 0.0072 | 0.8910 | 0.0540 | 18.3 | 0.0117 |
| 2006/349 | 11:38–17:31 | 317.4 | 2.37 | 0.05 | 2.45 | −0.08 | −1.60 | 0.43 | 0.0180 | 0.0055 | 0.8656 | 0.0414 | 16.5 | 0.0116 |
| 2007/019 | 20:57–23:56 | 1.4 | 2.18 | 0.07 | 2.177 | 0.003 | 0.04 | 1.23 | 0.0234 | 0.0055 | 0.8198 | 0.0420 | 20.0 | 0.0107 |
| Average: | — | — | 2.33 | 0.09 | — | −0.06 | −0.90 | 0.69 | 0.0184 | 0.0066 | 0.8605 | 0.0497 | 18.02 | 0.0119 |
| Scatter: | — | — | 0.09 | 0.02 | — | 0.04 | 0.63 | 0.32 | 0.0032 | 0.0011 | 0.0257 | 0.0086 | 1.36 | 0.0008 |

stab. = stability.

st. dev. = standard deviation.

Pass 2007/019 was conducted using a different front-end (cryogenics and bias voltage circuitry).

Pass 2007/019 noise diode "canned" value from L. D'Addario, e-mail (JPL internal document), Jet Propulsion Laboratory, Pasadena, California, January 18, 2007.

The summary for the analysis of the lunar noise data for X-band RCP on the 6-m-diameter Antenna 1 is shown in Table 2. Notice that the default ND temperature value used for comparison for the first few passes (1.84 K) is from Weinreb.[13] The front-ends for Antennas 1 and 3 were switched on January 11, 2007. The data for the last pass in Table 2 (2007/019) were acquired using the front-end equipment relocated from Antenna 3. An ambient-load calibration was performed by D'Addario and Miyatake[14] on January 18, 2007, and the resulting achieved noise diode value is provided in Table 2 for pass 2007/019 (1.99 K). This agrees very well with the value obtained from the lunar noise temperature calibration data ($1.91 \pm 0.12$ K), the difference (−0.08 K) falling within the scatter of the measurements (0.12 K).

[13] S. Weinreb, op cit.

[14] L. D'Addario and H. Miyatake, op cit.

**Table 2. X-band RCP summary on Antenna 1 (6 m).**

| Pass | Time span, UTC | Lunar phase angle, deg | $T_{ND}$ mean, K | $T_{ND}$ scatter, K | $T_{ND}$ default, K | $T_{ND}$ error, K | $T_{ND}$ error/ scatter | Gain stab., % | CC mean | CC st. dev. | BC mean | BC st. dev. | $T_{equip}$, K | $\tau$ zenith |
|---|---|---|---|---|---|---|---|---|---|---|---|---|---|---|
| 2006/306 | 00:04–09:43 | 152.0 | 1.79 | 0.09 | 1.84 | −0.05 | −0.56 | 0.52 | 0.0160 | 0.0133 | 0.9053 | 0.0790 | 15.0 | 0.0126 |
| 2006/313 | 07:04–17:00 | 212.8 | 1.79 | 0.09 | 1.84 | −0.05 | −0.56 | 1.03 | 0.0195 | 0.0085 | 0.8611 | 0.0610 | 16.0 | 0.0128 |
| 2006/320 | 11:36–13:57 | 330.0 | 1.88 | 0.11 | 1.84 | 0.04 | 0.36 | 0.29 | 0.0200 | 0.0134 | 0.8685 | 0.0880 | 15.0 | 0.0117 |
| 2006/321 | 18:53–21:46 | 343.6 | 1.92 | 0.1 | 1.84 | 0.08 | 0.80 | 0.48 | 0.0202 | 0.0146 | 0.8652 | 0.0980 | — | — |
| 2006/336 | 01:47–07:47 | 161.1 | 1.79 | 0.06 | 1.84 | −0.05 | −0.83 | 0.45 | 0.0228 | 0.0265 | 0.8372 | 0.1870 | — | — |
| 2006/342 | 08:34–15:56 | 203.8 | 1.83 | 0.08 | 1.84 | −0.01 | −0.13 | 0.95 | 0.0185 | 0.0110 | 0.9100 | 0.0520 | 15.0 | 0.0103 |
| 2006/349 | 11:38–17:31 | 317.4 | 1.91 | 0.14 | 1.84 | 0.07 | 0.50 | 0.65 | 0.0196 | 0.0180 | 0.8628 | 0.1270 | 14.0 | 0.0116 |
| 2007/019 | 20:57–23:56 | 1.4 | 1.91 | 0.12 | 1.99 | −0.08 | −0.67 | 0.19 | 0.16 | 0.0397 | 0.9567 | 0.1076 | — | — |
| Average: | — | — | 1.85 | 0.10 | — | −0.01 | −0.13 | 0.57 | 0.0191 | 0.0181 | 0.8834 | 0.1000 | 15.0 | 0.0118 |
| Scatter: | — | — | 0.06 | 0.02 | — | 0.06 | 0.62 | 0.30 | 0.0023 | 0.0103 | 0.0381 | 0.0427 | 0.7 | 0.0010 |

stab. = stability.

st. dev. = standard deviation.

Pass 2007/019 was conducted using a different front-end (cryogenics and bias voltage circuitry).

Pass 2007/019 noise diode "canned" value from L. D'Addario, e-mail (JPL internal document), Jet Propulsion Laboratory, Pasadena, California, January 18, 2007.

Pass 2006/336, glitch point at 5:40:23 UTC removed.

The summary for the analysis of the lunar noise data for Ka-band LCP on the 6-m-diameter Antenna 1 is shown in Table 3. Notice that the ND temperature default value used for comparison for the first few passes (2.08 K) is from Weinreb.[15] There was a significant 0.5-K bias in the estimated diode temperatures relative to the canned-in value for the first several passes before the front-ends were switched between Antennas 1 and 3. The front-ends for Antennas 1 and 3 were switched on January 11, 2007. The data for the last pass in Table 3 (2007/019) were acquired using the front-end equipment relocated from Antenna 3. An ambient-load calibration was performed by D'Addario and Miyatake[16] on January 18, 2007, and the resulting achieved noise diode value is provided (1.87 K). This value agrees very well with the value obtained from the lunar noise temperature calibration data ($1.85 \pm 0.13$ K), the difference (−0.02 K) falling well within the scatter of the measurements (0.13 K).

As far as Antenna 3 (12-m diameter) Ka-band LCP is concerned, there was evidence of feed horn issues causing significant asymmetry of the antenna pattern. In addition, there were also thermal daytime distortion issues during the passes. Earlier passes were plagued by thermal distortion issues on the surface of the dish, especially during passes where data were acquired in daylight. Thus, it was difficult to get a suitable model to account for these effects. There seemed to be a stable period at night between 3 a.m. and 6 a.m. local time where the efficiency approaches design expectations. This variation in antenna performance is beyond the model provided by Imbriale.[17] It is emphasized that the current study was done for a fixed subreflector position, prior to the installation of the subreflector axial motion system

[15] S. Weinreb, op cit.

[16] L. D'Addario and H. Miyatake, op cit.

[17] W. Imbriale, op cit.

**Table 3. Ka-band LCP summary on Antenna 1 (6 m).**

| Pass | Time span, UTC | Lunar phase angle, deg | $T_{ND}$ mean, K | $T_{ND}$ scatter, K | $T_{ND}$ default, K | $T_{ND}$ error, K | $T_{ND}$ error/ scatter | Gain stab., % | CC mean | CC st. dev. | BC mean | BC st. dev. | $T_{equip}$, K | $\tau$ zenith |
|---|---|---|---|---|---|---|---|---|---|---|---|---|---|---|
| 2006/306 | 00:04–09:43 | 152.01 | 2.70 | 0.16 | 2.08 | 0.62 | 3.88 | 1.12 | 0.0280 | 0.0166 | 0.8205 | 0.1080 | 9.0 | 0.0679 |
| 2006/313 | 07:04–17:00 | 212.76 | 2.60 | 0.16 | 2.08 | 0.52 | 3.25 | 0.55 | 0.0218 | 0.0249 | 0.8460 | 0.1770 | 10.0 | 0.0705 |
| 2006/320 | 11:36–13:57 | 330.03 | 2.34 | 0.11 | 2.08 | 0.26 | 2.36 | 1.15 | 0.0268 | 0.0147 | 0.8427 | 0.0008 | 11.0 | 0.0490 |
| 2006/321 | 18:53–21:46 | 343.62 | 2.39 | 0.15 | 2.08 | 0.31 | 2.07 | 0.45 | 0.0239 | 0.0279 | 0.8565 | 0.1690 | — | — |
| 2006/336 | 01:47–07:47 | 161.1 | 2.78 | 0.14 | 2.08 | 0.70 | 5.00 | 0.58 | 0.0187 | 0.0125 | 0.8814 | 0.0790 | — | 0.0414 |
| 2006/342 | 08:34–15:56 | 203.8 | 2.60 | 0.13 | 2.08 | 0.52 | 4.00 | 0.15 | 0.0221 | 0.0110 | 0.8452 | 0.0770 | 12.0 | 0.0380 |
| 2006/349 | 11:38–17:31 | 317.4 | 2.58 | 0.15 | 2.08 | 0.50 | 3.33 | 0.82 | 0.0184 | 0.0184 | 0.8851 | 0.1140 | 10.0 | 0.0540 |
| 2007/019 | 20:57–23:56 | 1.4 | 1.85 | 0.13 | 1.87 | −0.02 | −0.15 | 0.22 | 0.0271 | 0.0258 | 0.8836 | 0.1111 | 20.0 | 0.0447 |
| Average: | — | — | 2.46 | 0.14 | — | 0.43 | 2.97 | 0.63 | 0.0233 | 0.0190 | 0.8576 | 0.1045 | 12.0 | 0.0522 |
| Scatter: | — | — | 0.29 | 0.02 | — | 0.23 | 1.57 | 0.38 | 0.0037 | 0.0064 | 0.0236 | 0.0557 | 4.0 | 0.0127 |

stab. = stability.

st. dev. = standard deviation.

Pass 2007/019 was conducted using a different front-end (cryogenics and bias voltage circuitry).

Pass 2007/019 noise diode "canned" value from L. D'Addario, e-mail (JPL internal document), Jet Propulsion Laboratory, Pasadena, California, January 18, 2007.

Pass 2006/306, deleted data prior to 01:51 UTC for gain calculation.

used to characterize the thermal performance of the antenna. As a result, we expect that some of these data may not have been acquired with the antenna at optimum efficiency. Since the construction of this technique assumes that the antenna is operating nominally, this will introduce some error in the resulting $T_{ND}$ at Ka-band.

An example of system noise temperature data versus elevation angle for several tip curves repeated throughout pass 2006/306 for the 12-m antenna at Ka-band is shown in Fig. 12. Here, the antenna elevation angle spanned the range from 20 deg to 80 deg in steps of 10 deg. These data provide an estimate of equipment temperature ($T_{equip}$) which could include spillover and RFI, and $\tau$, the zenith optical depth of the atmosphere (using a single layer model). In Fig. 12, we see the effect of scatter during this pass, which lasted over 9 hours. The scatter at the lowest elevation angle (20 deg) is much larger than the scatter at other elevation angles, as expected. The model (red curve) fits the data reasonably well for this case, suggesting that the variations at each elevation angle are likely due to time-dependent changes in the atmosphere.

For some cases, the tip curves did not necessarily follow the expected atmospheric signature. Figure 13 displays one of the complications inherent with this method when the measurements may be corrupted by spillover or RFI. A more linear signature of system noise temperature with station elevation angle was observed at X-band for the 6-m-diameter antennas, necessitating a fit of the data as shown, used to model out the elevation-dependent signature in the analysis of Section IV in place of the atmospheric elevation-dependent model. Thus, in this case, the periodic tip curves performed during the pass were useful in characterizing the elevation-dependent cold-sky system noise temperature, which includes land-mask and RFI contributions.

The results of horizontal (equal-elevation angle slices) scans are shown in Fig. 14 (X-band RCP Antenna 1) and Fig. 15 (Ka-band LCP Antenna 1). Clearly, there are non-atmospheric features present at

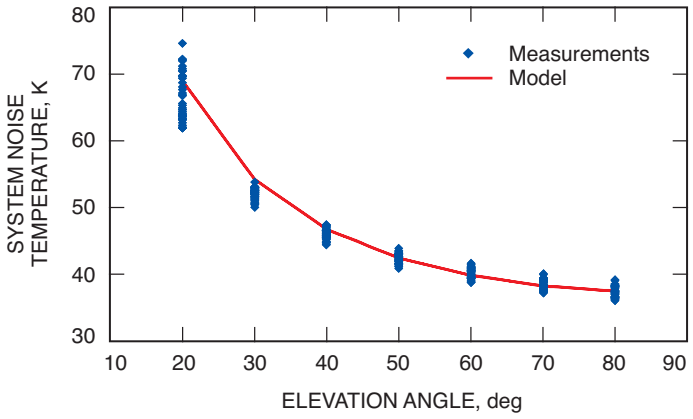


**Fig. 12. 2006/306 (November 2, 2006) tip curves for Ka-band on the 12-m antenna.**

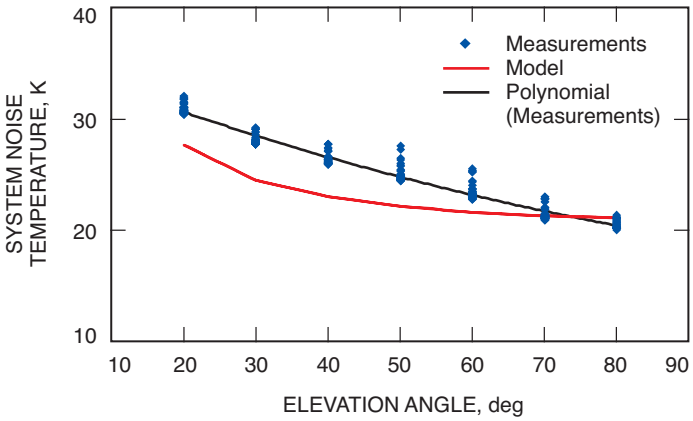


**Fig. 13. 2006/306 (November 2, 2006) tip curves for X-band RCP on 6-m Antenna 1.**

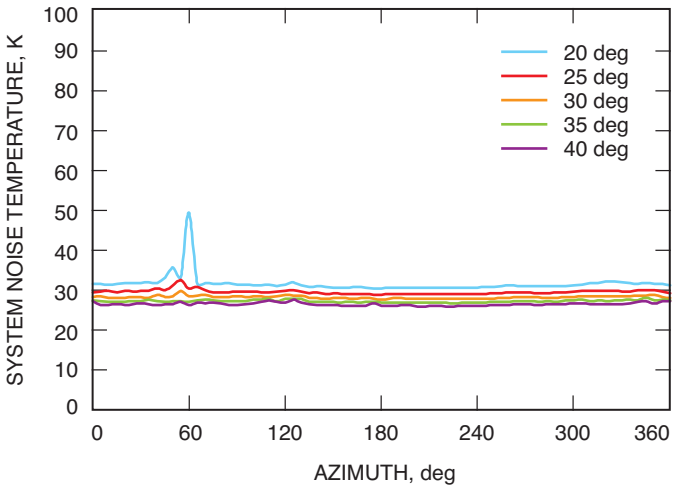


**Fig. 14. Land mask measurements performed on 2006/307 on X-band RCP Antenna 1 for different elevation angle cuts.**

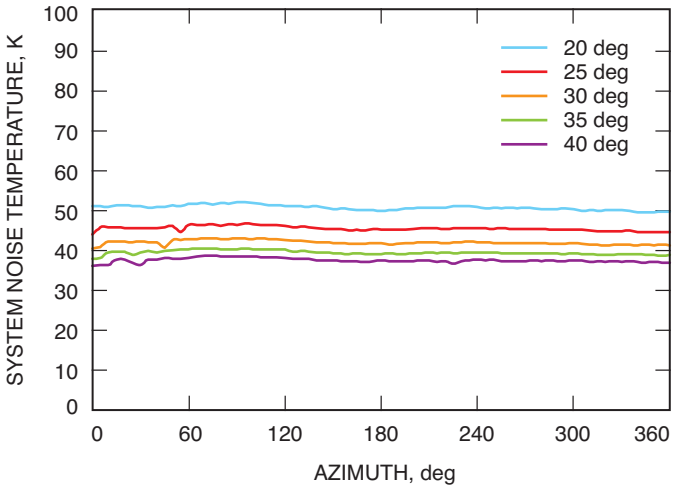


**Fig. 15. Land mask measurements performed on 2006/307 on Ka-band LCP Antenna 1 for different elevation angle cuts.**

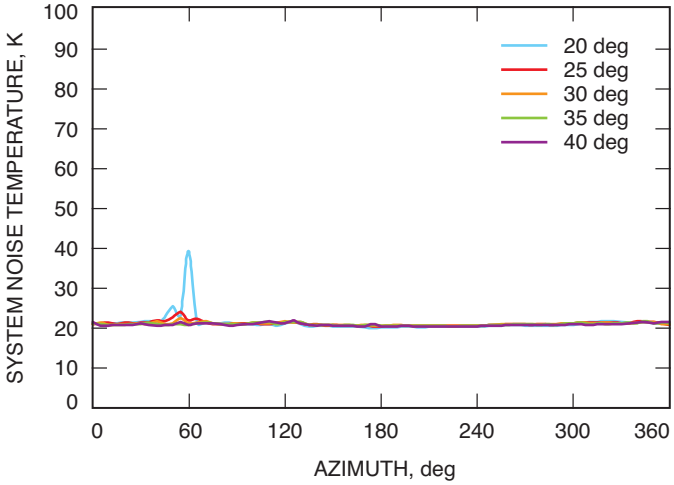


**Fig. 16. Land mask measurements performed on 2006/307 on X-band RCP Antenna 1 for different elevation angle cuts after removing an atmospheric model.**

X-band, as seen in Fig. 14. Figure 16 displays the data of Fig. 14 after removing an atmospheric model. Non-tropospheric effects are clearly evident in the data of Fig. 16 around azimuths of 40 to 60 deg at low elevation angles. The Ka-band curves are consistent with varying elevation-dependent atmospheric contributions riding on top of near-constant equipment temperature and cosmic background contributions, and hence suggest negligible RFI and land-mask contributions.

## VI. Conclusion

A calibration method has been presented that utilizes the Moon as an "ambient load" for antennas of a potential large array, where periodic conventional ambient-load techniques may not be practical on a quick turn-around basis. This approach of using the Moon as a calibration load is a big cost saver in hardware as well as in labor over the conventional method, where one would have to place absorber loads

over many antenna feeds. The details of this approach have been presented, as well as the theoretical background and measurements that illustrate the usefulness and limitations of this technique.

This calibration method can be used to measure the equivalent noise temperature contribution of the noise diodes. For the breadboard array, the values of the noise diode temperatures are used in the conversion of synchronous detector output voltages to system noise temperature. This technique can also be used to infer the consistency of other parameters such as the equivalent temperature of the back-end equipment as seen at the input to the LNA. All three breadboard antennas were calibrated concurrently using a script file, demonstrating its potential use in the case of a large array of many antennas per complex. This method could also be used as a system integration test to verify the optics and pointing performance of the antenna system.

## Acknowledgments

We acknowledge the assistance of numerous people of the array team who have provided support. We also appreciate the comments and suggestions provided by Larry D'Addario, Stephen Slobin, and Dayton Jones in the review of this article.

## References

[1] M. S. Gatti, "The Deep Space Network Large Array," *The Interplanetary Network Progress Report*, vol. 42-157, Jet Propulsion Laboratory, Pasadena, California, pp. 1–9, May 15, 2004. http://ipnpr/progress_report/42-157/157O.pdf

[2] S. Shambayati, D. Morabito, J. Border, F. Davarian, D. Lee, R. Mendoza, M. Britcliffe, and S. Weinreb, "Mars Reconnaissance Orbiter Ka-band (32 GHz) Demonstration: Cruise Phase Operations," *Proceedings of SpaceOps Conference*, American Institute of Aeronautics and Astronautics, Rome, Italy, June 23, 2006.

[3] N. Skou, *Microwave Radiometer Systems, Design, and Analysis*, Norwood, Massachusetts: Artech House, 1989.

[4] G. Evans and C. W. McLeish, *RF Radiometer Handbook*, Dedham, Massachusetts: Artech House, 1977.

[5] C. T. Stelzried, *The Deep Space Network—Noise Temperature Concepts, Measurements, and Performance*, JPL Publication 82-33, Jet Propulsion Laboratory, Pasadena, California, September 15, 1982.

[6] J. D. Kraus, *Radio Astronomy*, New York: McGraw-Hill, 1966.

[7] S. J. Keihm, "Interpretation of the Lunar Microwave Brightness Temperature Spectrum: Feasibility of Orbital Heat Flow Mapping," *Icarus*, vol. 60, pp. 568–589, 1984.

[8] S. J. Keihm and M. G. Langseth, "Lunar Microwave Brightness Temperature Observations Reevaluated in the Light of Apollo Program Findings," *Icarus*, vol. 24, pp. 211–230, 1975.

[9] D. D. Morabito, "Lunar Noise-Temperature Increase Measurements at S-Band, X-Band, and Ka-Band Using a 34-Meter-Diameter Beam-Waveguide Antenna," *The Interplanetary Network Progress Report*, vol. 42-166, Jet Propulsion Laboratory, Pasadena, California, pp. 1–18, August 15, 2006. http://tmo/progress_report/42-166/166C.pdf

[10] W. A. Imbriale, "Computing the Noise Temperature Increase Caused by Pointing DSS 13 at the Center of the Moon," *The Interplanetary Network Progress Report* vol. 42-166, Jet Propulsion Laboratory, Pasadena, California, pp. 1–10, August 15, 2006. http://tmo/progress_report/42-166/166E.pdf

[11] D. J. Rochblatt and B. L. Seidel, "Performance Improvement of DSS-13 34-Meter Beam-Waveguide Antenna Using the JPL Microwave Holography Methodology," *The Telecommunications and Data Acquisition Progress Report 42-108, October–December 1991*, Jet Propulsion Laboratory, Pasadena, California, pp. 253–270, February 15, 1992. http://ipnpr/progress_report/42-108/108S.PDF

[12] W. A. Imbriale and R. Abraham, "Radio Frequency Optics Design of the Deep Space Network Large Array 6-Meter Breadboard Antenna," *The Interplanetary Network Progress Report*, vol. 42-157, Jet Propulsion Laboratory, Pasadena, California, pp. 1–8, May 15, 2004. http://ipnpr/progress_report/42-157/157E.pdf

[13] W. A. Imbriale, "Radio Frequency Optics Design of the 12-Meter Antenna for the Array-Based Deep Space Network," *The Interplanetary Network Progress Report*, vol. 42-160, Jet Propulsion Laboratory, Pasadena, California, pp. 1–9, February 15, 2005. http://ipnpr/progress_report/42-160/160B.pdf

[14] R. Navarro and J. Bunton, "Signal Processing in the Deep Space Array Network," *The Interplanetary Network Progress Report*, vol. 42-157, Jet Propulsion Laboratory, Pasadena, California, pp. 1–17, May 15, 2004. http://ipnpr/progress_report/42-157/157N.pdf

[15] C. T. Stelzried and M. J. Klein, "Precision DSN Radiometer Systems: Impact on Microwave Calibrations," *Proceedings of the IEEE*, vol. 82, pp. 776–787, May 1994.

[16] J. D. Giorgini and the JPL Solar System Dynamics Group, "Horizons On-Line Ephemeris Computation System," Jet Propulsion Laboratory, Pasadena, California, 2007. http://ssd.jpl.nasa.gov/?horizons

[17] J. D. Giorgini and D. K. Yeomans, "On-Line System Provides Accurate Ephemeris and Related Data," *NASA Tech Briefs*, NPO-20416, p. 48, October 1999.

[18] J. D. Giorgini, D. K. Yeomans, A. B. Chamberlin, P. W. Chodas, R. A. Jacobson, M. S. Keesey, J. H. Lieske, S. J. Ostro, E. M. Standish, and R. N. Wimberly, "JPL's On-Line Solar System Data Service," *Bulletin of the American Astronomical Society*, vol. 28, no. 3, p. 1158, 1996.